Journal of Harbin Engineering University
ISSN: 1006-7043

Vol 44 No.12
December 2023

Digital Study of the Thermal Performance of a Microchannel, Cooled with a Cu-Water Nanofluid

A.Mekroud[1], Y.Kaabar[2]
[1] Institute of Applied Technical Sciences (ISTA),
Laboratory of Renewable Energy and Sustainable Development (LERDD),
University of the brothers MENTOURI Constantine
[2] School Polytechnic University
[3] Constantine, Algeria

Abstract
Geometry on the thermal performance of the microchannelare studied. It was observed that the increase in heat transfer is possible using the nanofluid compared to the base fluid. The heat transfer rate increases with the increase of the inlet velocity as well as the increase of the solid volume A numerical study of the thermal performance of a micro channel, cooled with pure water or with a Cu-water nano fluid was presented. The micro channel is partially maintained at a constant temperature. The continuity, momentum and energy equations are solved using a FLUENT code based on the finite volume method. The SIMPLE algorithm is used to bypass the velocity/pressure coupling. The thermal conductivity of the nanofluid is determined by the model of Patel et al [1]. The effects of relevant parameters such as Reynolds number, inlet effects, solid volume fraction and problem fraction of the nano fluid.

Keywords: simulation, micro channel, heat transfer, convection, Nano fluid, volume fraction, Reynolds number, Nusselt number.

1. Introduction

For reliable operation in industrial applications and electronic equipment. Indeed, the reliability of a system depends considerably on its operating temperature. For this, microchannels have been the subject of particular attention, especially for cooling devices used in the electronic, automotive and aerospace industries... The optimal design of microchannels improves their reliability and thermal performance.

The presentation of the geometries used in this study and the mathematical model containing the different equations governing this mode of heat transfer, as well as the boundary conditions of the physical model. The explanation of the finite volume method (MVF) and the different steps carried out for the numerical resolution by the FLUENT calculation code. The presentation, interpretation and discussion of the results obtained. Indeed, three effects are studied, first the effect of Reynolds number, the second includes the effect of the volume fraction and the third concerns the effect of adding ribs to the heated walls.

2. Mathematical Model And Geometry

Figure 1 considers a two-dimensional horizontal microchannel . The microchannel has a hydraulic $2h = 50\mu m$length $l = 2.5mm$and diameter . The equivalent values in dimensionless are dimensionless length and $L = l/h = 100$dimensionless $H = h/h = 1$width . The length of the microchannel is divided into three parts with lengths$l_1 = 0.75mm$ (input), $l_2 = 1mm$(middle) and $l_3 = 0.75mm$(output). The inlet section ($L_1 = l_1/h = 30$) and outlet ($L_3 = l_3/h = 30$) are thermally insulated. The middle section $L_2 = l_2/h = 40$is heated to a temperature T_H =303 K. The cooling fluid enters the microchannel at a temperature T_C =293 K, it is considered either pure water or nanofluid .

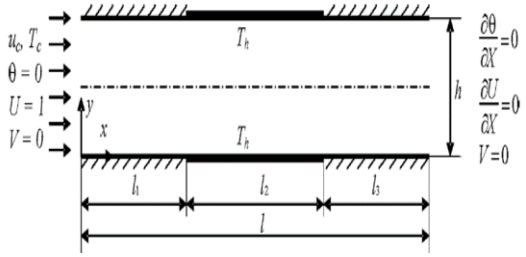

Figure 1: Schematic diagram of the physical model

The nanofluid contains water and Cu nanoparticles which are in thermal equilibrium. Suspended copper nanoparticles are assumed to have uniform size and shape and to be spherical. The nanofluid is considered Newtonian and incompressible, the flow in the microchannel is laminar. The effects of radiation are neglected. The thermophysical properties of the nanofluid are considered constant. At a temperature of 25 °C, the thermophysical properties of pure water (base fluid) and Cu nanoparticles are presented in the following table.

Table Error! No text of specified style in document.**. 1: Thermophysical properties of pure water and Cu at 25 °C [8] .**

	Eau pure	Cu
Pr	6,2	-
ρ (kg.m^{-3})	997.1	8933
Cp (J.kg^{-1}.K^{-1})	4179	385
k (W.m^{-1}.K^{-1})	0,613	400
β (K^{-1})	21 × 10^{-5}	1,67 × 10-5
α (m^2.s^{-1})	1,47 × 10^{-7}	1163,1 × 10^{-7}

Thermophysical properties of nanofluids

The addition of nanoparticles in a base fluid considerably changes the thermophysical properties of fluids including thermal conductivity, dynamic and kinematic viscosity, thermal capacity and density. The change in thermophysical properties is related to several parameters, for example particle concentration, particle material, particle size and conductivity of the base fluid.

The volume fraction (ϕ)

The volume fraction can be represented as follows:

$$\varphi == \frac{V_p}{V_p + V_f} \quad (1)$$

Density ($\boldsymbol{\rho_{nf}}$)

We estimate the value of the density of the nanofluids from the mixing law.

$$\rho_{nf} = \left(\frac{m}{V}\right)_{nf} = \frac{m_f + m_p}{V_f + V_P} = \frac{\rho_f V_f + \rho_p V_p}{V_T} = \rho_f(1 - \varphi) + \rho_p \varphi \quad (2)$$

Thermal conductivity of nanofluids ($\boldsymbol{k_{nf}}$)

Numerous experimental and theoretical researches have been carried out to velop models estimating the value of the conductivity of nanofluids depends on several parameters such as the volume fraction, the size and shape of the nanoparticles, the nature of the particles and the base fluid.

- **Patel et al model** [1]

The model proposed by Patel et al seems better approximate with certain experimental results compared to other models for the case of spherical nanoparticles with no limitation concerning the concentrations of the nanoparticles. This model is expressed by:

$$\frac{k_{eff}}{k_f} = 1 + \frac{k_p A_p}{k_f A_f} + c_p k_p Pe \frac{A_p}{k_f A_f} \quad (4)$$

Such as : $Pe = \frac{u_p d_p}{\alpha_f}$ (5)

$$u_p = \frac{2k_b T}{\pi \mu_f d_p^2} \quad (6)$$

$$\frac{A_p}{A_f} = \frac{d_f}{d_p} \frac{\varphi}{(1-\varphi)} \quad (7)$$

We replace equations (5,6 and 7),) in equation (4), we find the equation$suivante$:

$$k_{eff} = k_f + k_p \frac{d_f \phi}{dp(1-\phi)} \left(1 + \frac{2cTk_b}{\pi \mu_f d_p \alpha_f}\right) \quad (8)$$

The thermal conductivity of the nanofluids in our work was calculated from the model of Patel et al. [1]

Dynamic viscosity ($\boldsymbol{\mu_{nf}}$)

We will present some models widely used in the case of nanofluids .

Brinkman model [19] describes a non-linear evolution of dynamic viscosity with volume fraction.

$$\mu_{nf} = \frac{\mu_f}{(1-\varphi)^{2.5}} \quad (9)$$

2.1. Simplifying assumptions

The simplifying assumptions of our study are:

- The fluid is Newtonian and incompressible
- Thermophysical properties of fluid are constant
- Heat transfer by radiation is neglected.
- Flow regime is laminar and stationary
- Two-dimensional flow (following Cartesian coordinates x and y)
- Continuous medium
- The nanoparticles are assumed to have uniform shape and size and to be spherical

- We neglect the phenomenon of buoyancy of nanoparticles
- The fluid and the nanoparticles are in thermal equilibrium
- There is no chemical reaction
- Viscous dissipation is negligible

2.2. Mathematical model

The dimensional equations in steady state and in a single-phase model can be written as follows, taking into account all the hypotheses:

Adimensionalization of equations

We move from the dimensional form to the non-dimensional form to reduce the number of parameters and in order to find general solutions. It also simplifies the resolution of systems of equations.

Continuity equation :

$$\frac{\partial U}{\partial X}+\frac{\partial V}{\partial Y}=0 \quad (16)$$

Equation of momentum along the axis (X) :

$$U\frac{\partial U}{\partial X}+V\frac{\partial U}{\partial Y}=-\frac{\partial P}{\partial X}+\frac{1}{Re}\frac{\mu_{nf}}{\rho_{nf}\nu_f}\left[\frac{\partial^2 U}{\partial X^2}+\frac{\partial^2 U}{\partial Y^2}\right] \quad (17)$$

Momentum equation along the Y axis:

$$\boldsymbol{U\frac{\partial V}{\partial X}+V\frac{\partial V}{\partial Y}=-\frac{\partial P}{\partial Y}+\frac{1}{Re}\frac{\mu_{nf}}{\rho_{nf}\nu_f}\left[\frac{\partial^2 V}{\partial X^2}+\frac{\partial^2 V}{\partial Y^2}\right]} \quad (18)$$

Energy equation

$$U\frac{\partial \theta}{\partial X}+V\frac{\partial \theta}{\partial Y}=\frac{\alpha_{nf}}{\alpha_f}\frac{1}{Re\,Pr}\left[\frac{\partial^2 \theta}{\partial X^2}+\frac{\partial^2 \theta}{\partial Y^2}\right] \quad (19)$$

The Nusseltlocalnumber (Nu) along the bottom wall can be expressed as follows:

$$Nu(X)=-\frac{k_{nf}}{k_f}\left(\frac{\partial \theta}{\partial Y}\right)_{Y=0} \quad (20)$$

average Nu_{moy}Nusselt number ( ) is determined by integrating the local Nusselt number (Nu)along the isothermal wall:

$$Nu_{moy}=\frac{1}{L_2}\int_{L_1}^{L_1+L_2} Nu(X)dX \quad (21)$$

Conditions to the limits

At the entrance to the canal:

$$X=\frac{x}{h}\ ;\ Y=\frac{y}{h}\ ;\ U=\frac{u}{u_\infty}$$

$$V=\frac{v}{u_\infty}\ ;\ P=\frac{p}{\rho_{nf}u_\infty^2}\ ;\ \theta=\frac{T-T_c}{T_h-T_c}$$

➢ **At the exit of the canal:**

To $x=l$ and$0\le y\le h$; $\frac{\partial u}{\partial x}=v=\frac{\partial T}{\partial x}=0$

C to d: to $X=L$ and$0\le Y\le 1$; $\frac{\partial U}{\partial X}=V=\frac{\partial \theta}{\partial X}=0$

➢ **With isothermal (heated) walls:**

To $y=0$and $y=h$and$l_1\le x\le l_2$;$u=v=0$, $T=T_H$

C to d: to $Y=0$and $Y=1$and $L_1\le X\le L_2$;$U=V=0$, $\theta=1.0$

➢ **At adiabatic walls:**

To $y=0$and $y=h$and $0\le x<l_1$ et $l_2<x\le l_3$;$u=v=0$,$\frac{\partial T}{\partial y}=0$

C to d: to $Y=0$and $Y=1$and $0\le X<L_1$ et $L_2<X\le L_3$;$U=V=0$,$\frac{\partial \theta}{\partial Y}=0$

3. Digital Resolution Model

For our numerical simulation, we used a FLUENT calculation code based on the finite volume method as a means of discretizing the equations managing the flow phenomenon . .

Validation of the calculation code

The validation is carried out by comparing the ratio of the average Nusselt numbers of the nanofluid and the base fluid $\left(\frac{Nu_{moy}}{Nu_{moy,f}}\right)$as well as the temperature profiles in different sections of the microchannel with the results obtained by Raisi et al [8] . The results show that the present study is in good agreement with the results of this one (figures 1 and 2).

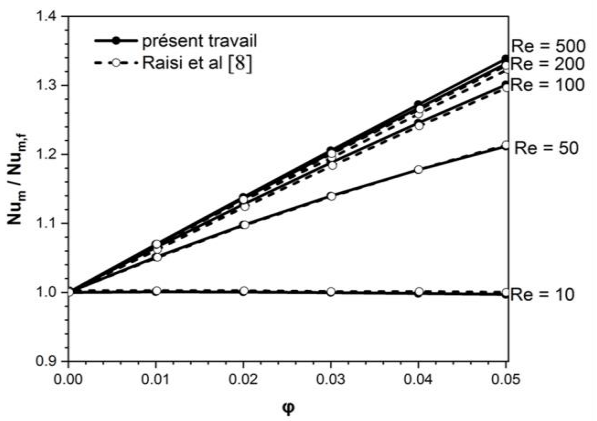

Figure. 2 : Ratio of the average Nusselt number as a function of the volume fraction for different Reynolds numbers

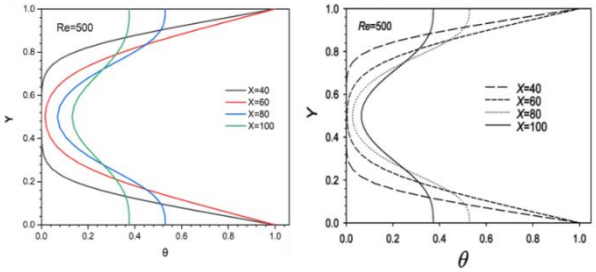

Figure 3 : Temperature profiles across different sections of the microchannel for Re = 500 and ϕ = 0.03

Reynolds number effect

In this section, we studied the effect of the variation of the Reynolds number for a laminar flow of nanofluid (water-Cu) of volume concentration ϕ = 0.03, the Reynolds numbers considered are Re = 10, 50, 100, 200 and 500.

In numerical simulations, to vary the Reynolds number, we vary the inlet speed.

Temperature field in the microchannel

Figure 3 shows the thermal field for different Reynolds numbers. The isotherms show that at Re $\theta = 1$)= 10 , the nanofluid temperature increases as the nanofluid moves through the heated section (L $_{1 \leq}$ in the exit section (L $_{2 \leq}$ flow, the establishment length of the thermal boundary layer is greater, temperature gradients remain along the microchannel therefore the heat exchange is greater when the Reynolds number is increased

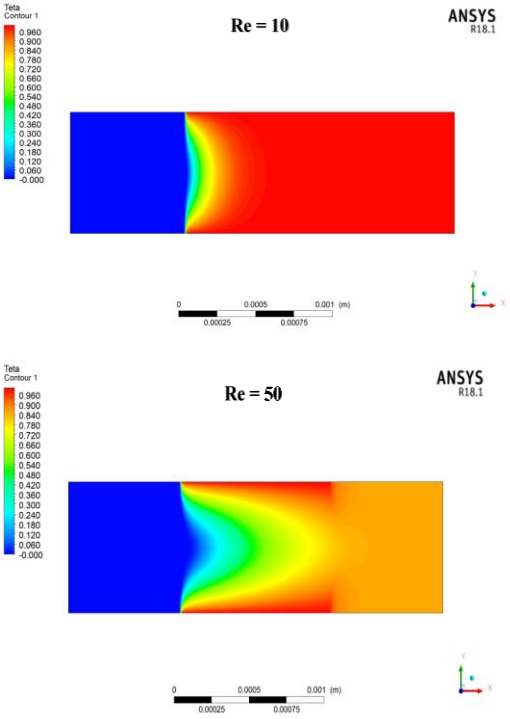

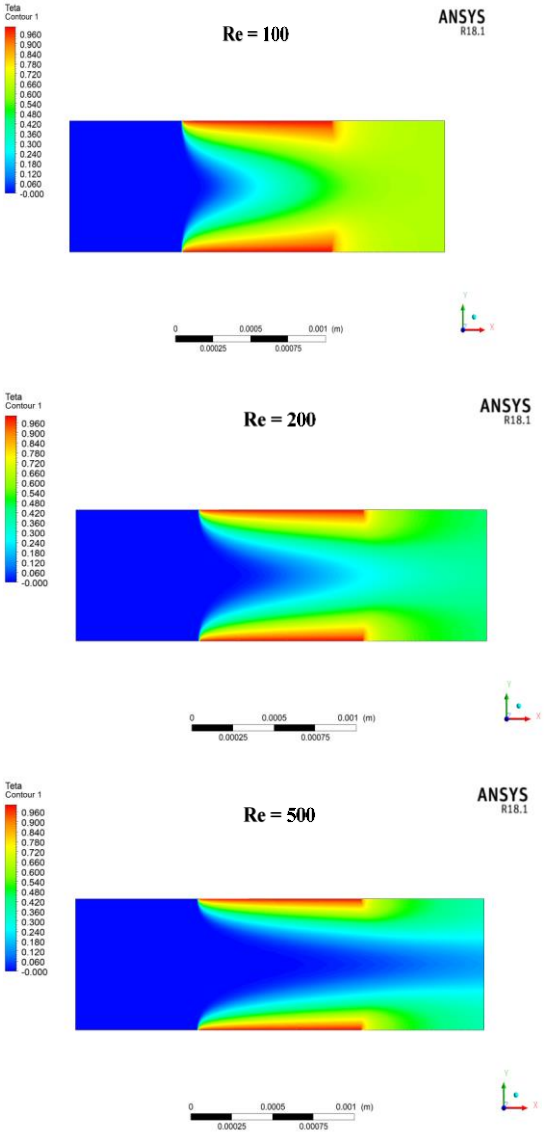

Figure 3-thermal field for different Re

Temperature variation in the center of the pipe

Figure 4 shows the temperature variation at the center of the microchannel for different Reynolds numbers. We notice that the temperature begins to increase as soon as it enters the heated section of the microchannel . For low Reynolds, the rate of this increase is higher. The reason for increasing the nanofluid temperature at low Reynolds is that there is sufficient time to exchange heat between the nanofluid and the walls of the microchannel .

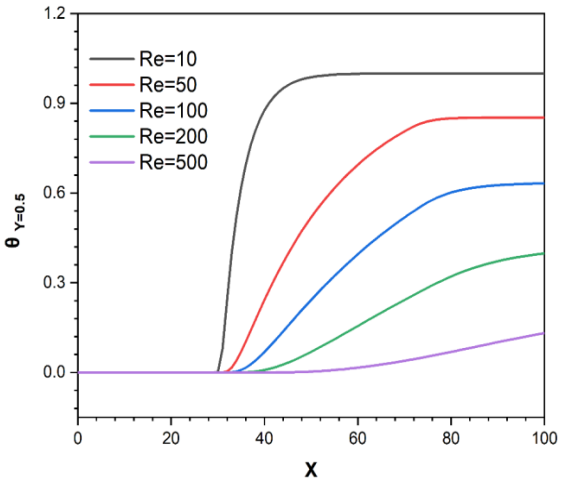

Figure 4 :Variation of the temperature at the center of the pipe for different Reynolds numbers with ϕ = 0.03

Temperature profiles across different sections of the microchannel

Figure 5 , illustrates the temperature profiles across different sections of the microchannel for different Reynolds numbers. We notice that at Re = 10, the temperature profiles of the nanofluid (ϕ = 0.03) are uniform in the different sections of the microchannel , except at X = 40. When we increase the Reynolds number up to Re = 50, a variation of the temperature profile at X = 60 is manifested. As the Reynolds number increases up to Re = 100, a significant variation is evident in the temperature profile across the microchannel sections , except at X = 100, where the temperature profile is almost uniform. The large Reynolds number values (at Re = 200 and Re = 500) result in a varied temperature profile in all the different sections of the microchannel . The reason for this behavior is the heat transfer rate between the nanofluid and the heated walls and again circulation speed of the nanofluid .

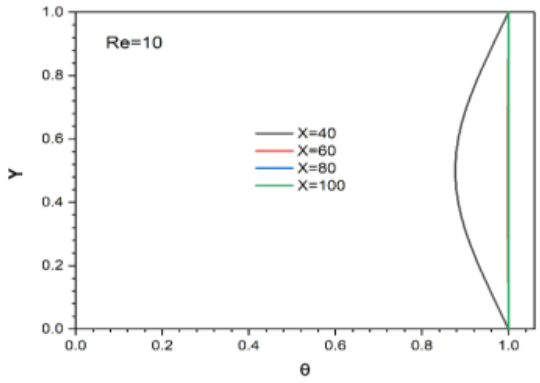

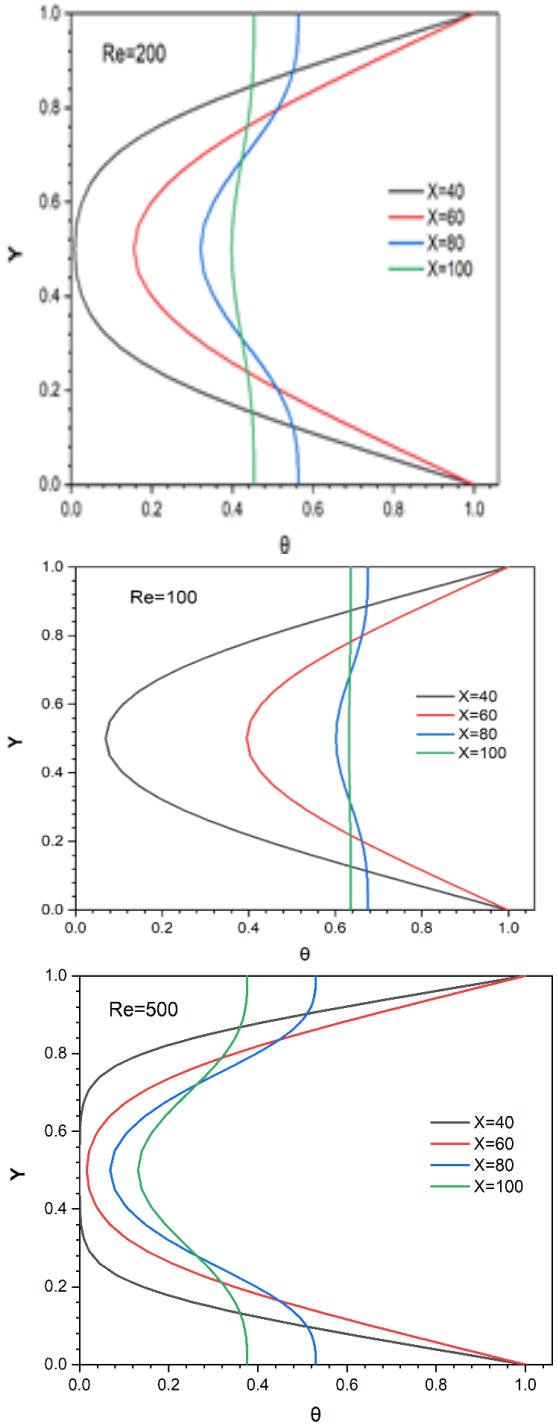

Figure 5: Temperature profiles across different sections of the microchannel for different Reynolds numbers with ϕ = 0.03

Effect of volume fraction

In this section, we studied the effect of volume concentration on the thermal and dynamic behavior of a laminar flow of nanofluid (water-Cu). For a Reynolds number Re = 100, the values of the volume fractions are ϕ = 0; 0.01; 0.02; 0.03; 0.04; 0.05.

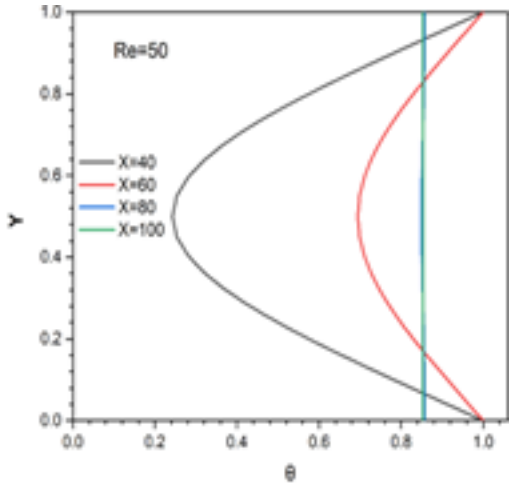

Figure 6 : Temperature profiles

In our case the effect of the volume fraction reflects the effect of the thermophysical properties of the nanofluid . The nanoparticles increase the thermal conductivity of the base fluid therefore they improve the heat transfer within the microchannel.

Temperature fields in the channel

Figure 7shows the thermal field of the nanofluid flow as a function of the volume fraction of the nanoparticles. It is noted that the nanofluid temperature increases with increasing volume fraction. So, the difference between the temperature of the isothermal walls and the temperature of the nanofluid will decrease. A comparison between the nanofluid isotherms for different volume fraction values indicates that the temperature of nanofluids with large volume fraction increases faster compared to low fractions. This behavior can be explained by the higher relative thermal conductivity when increasing the volume fraction.

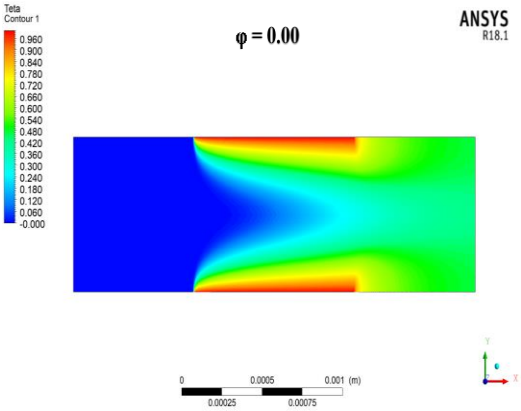

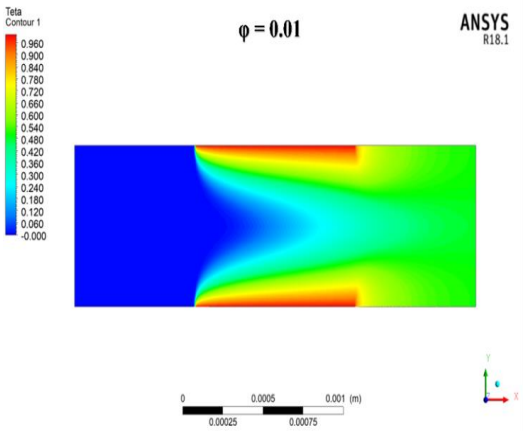

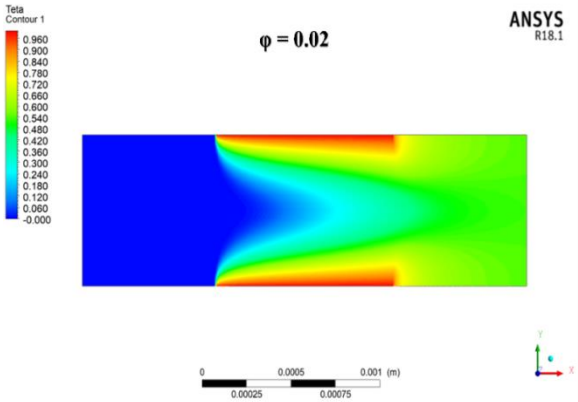

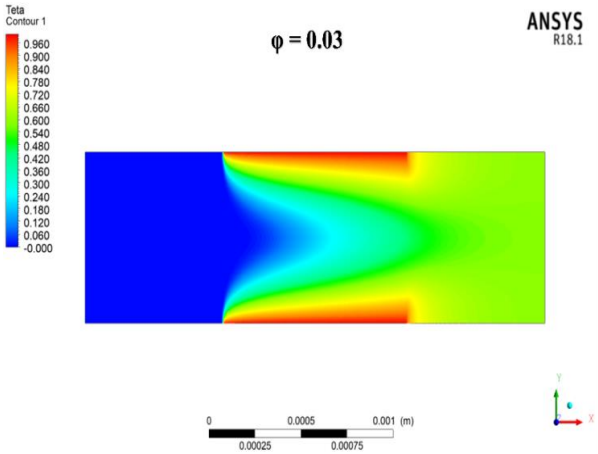

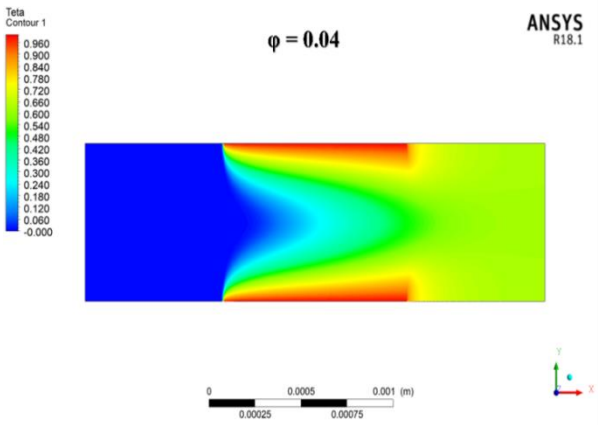

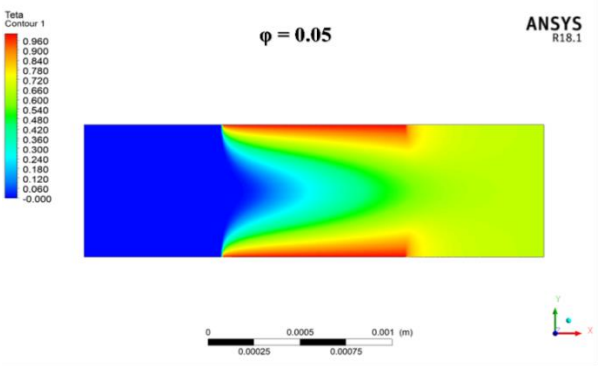

Figure.7: Temperature field for different volume fractions with Re = 100

Dimensionless temperature variation at the channel outlet

Figure 8shows the evolution of the dimensionless temperature at the exit of the microchannel for different volume fractions. We note that high temperatures are obtained for high volume fractions, the addition of nanoparticles increases the heat transfer between the isothermal walls and the nanofluid .

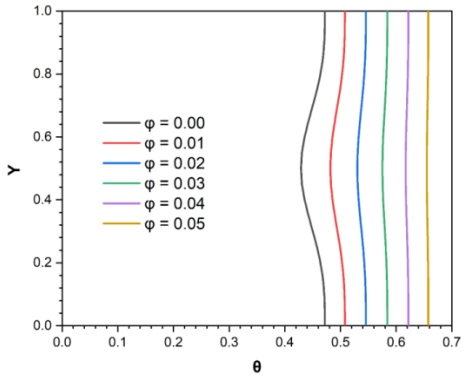

Figure 8: Variation of the dimensionless temperature at the channel outlet for different volume fractions with Re = 100

Variation of the average dimensionless temperature at the channel outlet

Figure ,9illustrates the variation of the average dimensionless temperature at the exit of the microchannel for different volume fractions. We note that the average dimensionless temperature at the outlet of the channel increases linearly with the increase in the volume fraction. The reason is the increase in heat transfer when adding nanoparticles.

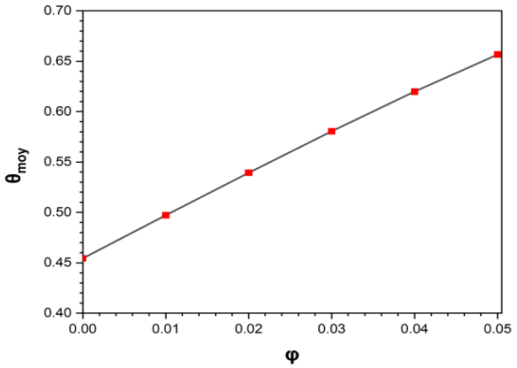

Figure 9: Variation of the average dimensionless temperature at the exit of the micro channel for different volume fractions with Re = 100

Variation of the local Nusselt number

Figure 10 shows the evolution of the local Nusselt number as a function of the volume fraction along the heated section. We notice that for the different volume fractions of the nanoparticles in suspension , the local Nusselt number decreases as a function of heated.

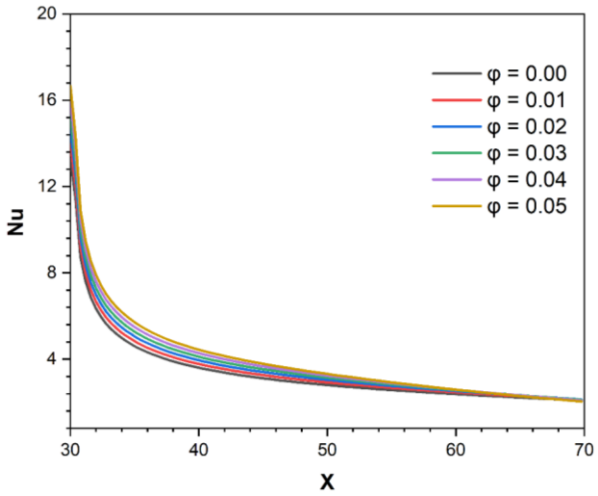

Figure Error! No text of specified style in document.**10 : Variation of the local Nusselt number for different volume fractions with Re = 100**

Effect of volume fraction as a function of variation in Reynolds number

Figure 11 shows the variation of the average Nusselt number as a function of the Reynolds number for different volume fractions. for Re = 10, the value of the average Nusselt number remains practically unchanged when the volume fraction is increased. However, a continued increase in the average Nusselt number is evident as the volume fraction is increased for higher values of the Reynolds number. This is due to the higher thermal

conductivity of the nanoparticles added to the base fluid.

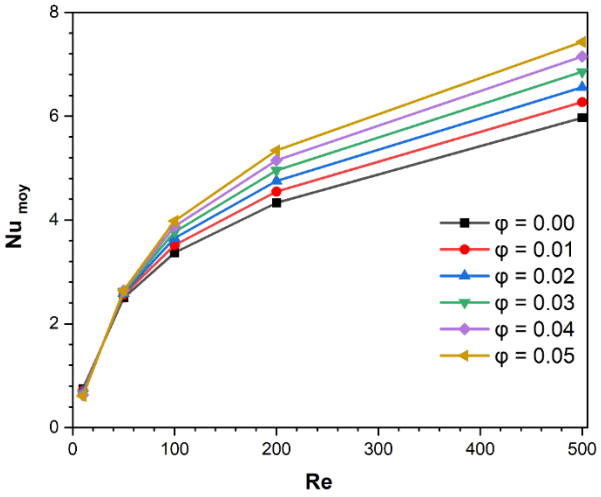

Figure. 11 : Variation of the average Nusselt number as a function of the Reynolds number for different volume fractions

According to the previous results and using the Excel tool, we can arrive at this correlation:

The results show that the present study is in good agreement with the results of Raisi et al. [8] .

Presence of ribs

Figure shows 10the temperature contours (isotherms) for rectangular, triangular and ribless ribs. It is noted that the different shapes of ribs along the flow positively affect the mixing of the nanofluid . Among all shapes tested, the evolution of these lines for triangular ribs indicates better flow mixing for these rib shapes.

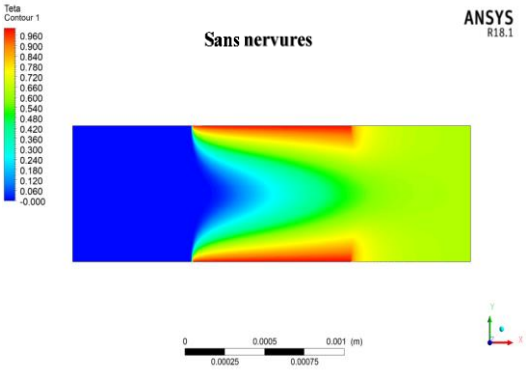

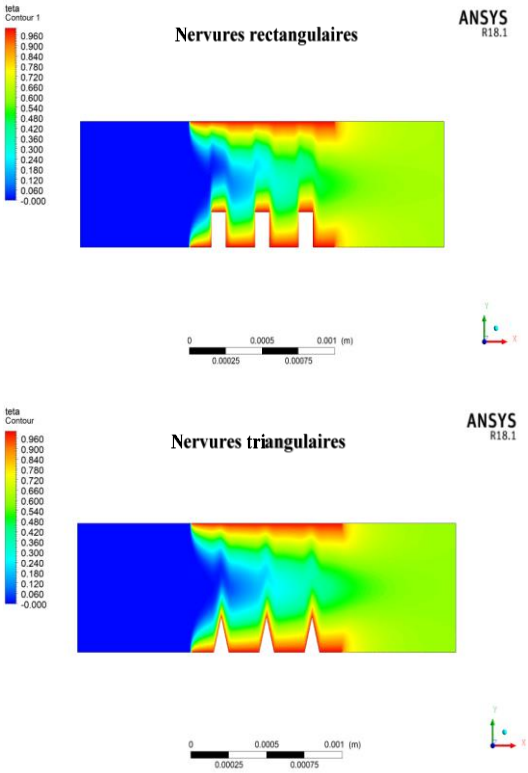

Figure Error! No text of specified style in document.**: Temperature field for different types of ribs with Re = 100 and ϕ = 0.03**

Contours of streamlines

Figure 11 , shows the velocity contours for different rib types. Using ribs with acute-angled surfaces results in specific changes in axial velocity contours. Due to the contacts between the nanofluid and the ribs, significant variations in axial velocity gradients and some small vortices occur. It is also noted that the highest speed gradient is achieved for the rectangular, triangular and ribless rib shapes respectively, which leads to significant changes in the speed. The variations become greater when the fluid meets the next corner of the rib.

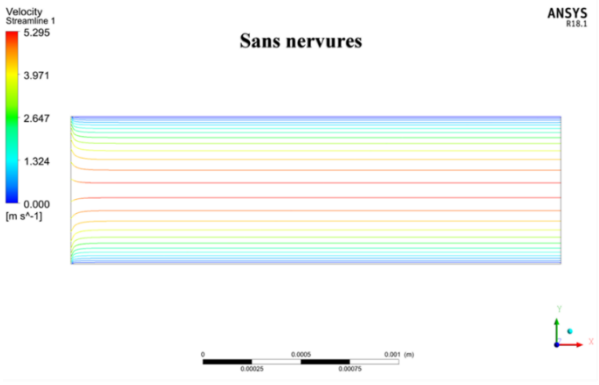

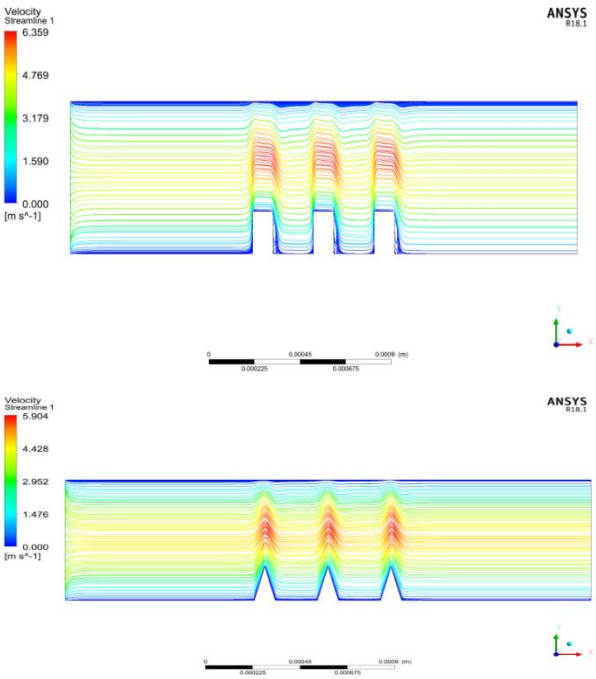

Figure 13 : Contours of streamlines for different types of ribs with Re = 100 and ϕ = 0.03

Variation of the local Nusselt number

Figure illustrates the local 12Nusselt number along the microchannel for ϕ = 0.03 and Re = 100 and for different rib shapes. We notice that the variation of the local Nusselt number depends on the shapes of the ribs. The maximum variations of the local Nusselt number are obtained with the rectangular shape of the ribs. Likewise the first rib allows a maximum variation of the local Nusselt number , through the following ribs, the variations become less and less important.

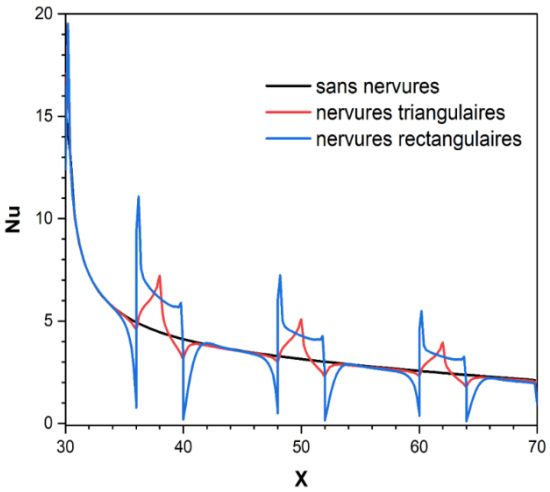

Figure 14 : Variation of the local Nusselt number for different types of ribs with Re = 100 and ϕ = 0.03

Previous results show that the present study is in good agreement with the results of Behnampouret al. [23]

Variation of the average Nusselt number as a function of the Reynolds number

Figure 13 shows the average Nusselt numberversus Reynolds number for different rib shapes. We notice that the rectangular shape has the highest average Nusselt number. Additionally, the triangular shape has a higher Nusselt number than the case without ribs. The reason is the abrupt variation of the velocity profile for the rectangular and triangular shape. For low Reynolds numbers, rectangular and triangular ribs behave similarly. When increasing the Reynolds number, the rectangular rib shape shows more efficient behavior and the heat transfer increases significantly with this rib shape. On the other hand, the results show that for all rib shapes, by increasing the inlet speed, the heat transfer and the number of nusselt increases significantly.

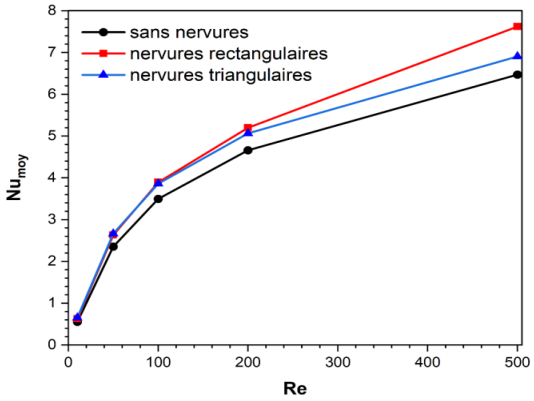

Figure 15 : Variation of the average Nusselt number as a function of the Reynolds number for different types of ribs

According to the previous results and using the Excel tool, we can arrive at these correlations:

- **Without ribs**

$$Nu_{moy} = 0.1492\ Re^{0.6024} \quad (22)$$

$$R^2 = 0.952 \quad (23)$$

- **Rectangular ribs**

$$Nu_{moy} = 0.1985\ Re^{0.6061} \quad (24)$$

$$R^2 = 0.9485 \quad (25)$$

- **Triangular ribs**

$$Nu_{moy} = 0.1985\ Re^{0.6061} \quad (26)$$

$$R^2 = 0.9485 \quad (27)$$

4. General Conclusion

In this simulation work we carried out a numerical study of heat transfer by forced convection in a

two-dimensional microchannel. The walls of the central section of the microchannel are maintained at a constant temperature. The microchannel is cooled by a nanofluid Cu-water .

The governing equations of continuity, momentum and energy are solved by the FLUENT CFD which is designed based on the finite volume method.

The flow and temperature fields as well as the heat transfer rate of the microchannel are studied for different Reynolds numbers, solid volume fractions and problem geometries. The Brownian motion of nanoparticles is taken into account in the model used to determine the thermal conductivity of nanofluids . The results of the numerical analysis lead to the following conclusions:

- For all Reynolds number values, the nanofluid flow grows very quickly before reaching the heated section of the microchannel . Increasing the Reynolds number results in a higher heat transfer rate.
- The heat transfer rate increases with volume fraction. This is due to the improved thermal performance due to the increased volume ratio of nanoparticles with relatively higher thermal conductivity. Additionally, a more notable increase in Nusselt number with volume fraction is evident at higher Reynolds numbers.
- Heat transfer is improved when ribs are added to the walls of the microchannel .

thermophysical properties of the nanofluid and the geometric parameters have a considerable effect on the heat exchange by forced convection.

In perspective, we recommend the numerical study of the sliding effect in a three-dimensional microchannel.

References

[1] HE Patel, T. Sundararajan, T. Pradeep, A. Dasgupta, N. Dasgupta, and SK Das, “A micro-convection model for thermal conductivity of nanofluids,” *Pramana – J. Phys.* , flight. 65, no. 5, pp. 863–869, 2005.

[2] A. Technologies, “heat dissipation in electronic components/systems,” LUSAC (University Laboratory of Applied Sciences of Cherbourg), 2015.

[3] KHENTOUL Moussa, “Numerical Study of Mixed Convection in a Horizontal Channel Containing Fins,” University of Mentouri Brothers - Constantine, 2016.

[4] M. Cristina and R. Almeida, “Study of two-phase flows for the cooling of electronic components in embedded systems,” Université Grenoble Alpes, 2019.

[5] G. Bachir, “Contribution to the study of natural convection in nanofluids in Rayleigh-Bénard configuration,” University Toulouse III- Paul Sabatier, 2010.

[6] S. KLALECHE and A. MADJOUR, “Numerical simulation of forced convection between two disks in the presence of a nanofluid,” Mouloud Mammeri University of Tizi-Ouzou, 2015.

[7] A. K. Santra, S. Sen, and N. Chakraborty, “Study of heat transfer due to laminar flow of copper-water nanofluid through two isothermally heated parallel plates,” *Int. J. Therm. Sci.*, vol. 48, no. 2, pp. 391–400, 2009, doi: 10.1016/j.ijthermalsci.2008.10.004.

[8] A. Raisi, B. Ghasemi, and S. M. Aminossadati, “A numerical study on the forced convection of laminar nanofluid in a microchannel with both slip and no-slip conditions,” *Numer. Heat Transf. Part A Appl.*, vol. 59, no. 2, pp. 114–129, 2011, doi: 10.1080/10407782.2011.540964.

[9] E. Manay and B. Sahin, “The effect of microchannel height on performance of nanofluids,” *Int. J. Heat Mass Transf.*, vol. 95, pp. 307–320, 2016, doi: 10.1016/j.ijheatmass transfer.2015.12.015.

[10] M. Izadi, M. M. Shahmardan, M. Norouzi, A. M. Rashidi, and A. Behzadmehr, “Cooling performance of a nanofluid flow in a heat sink microchannel with axial conduction effect,” *Appl. Phys. A Mater. Sci. Process.*, vol. 117, no. 4, pp. 1821–1833, 2014, doi: 10.1007/s00339-014-8760-1.

[11] M. Sheikholeslami, S. A. Farshad, Z. Ebrahimpour, and Z. Said, “Recent progress on flat plate solar collectors and photovoltaic systems in the presence of nanofluid: A review,” *J. Clean. Prod.*, vol. 293, p. 126119, 2021, doi: 10.1016/j.jclepro.2021.126119.

[12] S. Rashidi, M. Eskandarian, O. Mahian, and S. Poncet, “Combination of nanofluid and inserts for heat transfer enhancement: Gaps and

challenges," *J. Therm. Anal. Calorim.*, vol. 135, no. 1, pp. 437–460, 2019, doi: 10.1007/s10973-018-7070-9.

[13] I. Pak, B., C., et Cho, Y., "Hydrodynamic and heat transfer study of dispersed fluids with submicron metallic oxide particles," *Exp. Heat Transf.*, vol. 11, pp. 151–170, 1998.

[14] Y. Xuan and W. Roetzel, "Conceptions for heat transfer correlation of nanofluids," *Int. J. Heat Mass Transf.*, vol. 43, pp. 3701–3707, 2000.

[15] C. Maxwell., J., *A Treatise on Electricity and Magnetism*. U.K: Clarendon Press, 1881.

[16] K. Hamilton, R., L., et Crosser, O., "Thermal conductivity of heterogeneous two component systems," *Ind. Eng. Chem. Fundam.*, vol. 1, pp. 187–191, 1962.

[17] W. Yu and S. U. S. Choi, "The role of interfacial layers in the enhanced thermal conductivity of nanofluids : A renovated Maxwell model," *J. Nanoparticle Res.*, pp. 167–171, 2003.

[18] Einstein, "Eine Neue Bestimmung der Molekuldimensionen," *Ann. Phys. Leipzig*, vol. 19, pp. 289–306, 1906.

[19] H. C. Brinkman, "The Viscosity of Concentrated Suspensions and Solutions," *J. Chem. Phys.*, vol. 571, pp. 1–2, 1952, doi: 10.1063/1.1700493.

[20] G. K. Batchelor, "Brownian diffusion with hydrodynamic interaction," *J. Fluid Mech.*, vol. 74, no. 1, pp. 1–29, 1976.

[21] R. S. Vajjha, D. K. Das, and D. P. Kulkarni, "International Journal of Heat and Mass Transfer Development of new correlations for convective heat transfer and friction factor in turbulent regime for nanofluids," *Int. J. Heat Mass Transf.*, vol. 53, no. 21–22, pp. 4607–4618, 2010, doi: 10.1016/j.ijheatmasstransfer.2010.06.032.

[22] M. MOSTEFAI DELLA and I. HAMDI, "Study of the forced convection of a laminar flow in a horizontal channel using a nanofluid," Ecole nationale polytechnique de Constantine, 2018.

[23] A. Behnampour *et al.* , "Analysis of heat transfer and nano fl uid fl uid fl ow in microchannels with trapezoidal, rectangular and triangular shaped ribs," *Phys. E Low-dimensional Syst. Nanostructures* , vol. 91, no. April, pp. 15–31, 2017, doi: 10.1016/j.physe.2017.04.006.